Length scale formation in the Landau levels of quasicrystals

Junmo Jeon,[1,*] Moon Jip Park,[1,2,†] and SungBin Lee[1,‡]
[1]*Department of Physics, Korea Advanced Institute of Science and Technology, Daejeon 34141, South Korea*
[2]*Center of Theoretical Physics of Complex Systems, Institute for Basic Science (IBS) Daejeon 34126, Republic of Korea*

(Received 16 June 2021; accepted 25 January 2022; published 31 January 2022)

Exotic tiling patterns of quasicrystals have motivated extensive studies of quantum phenomena such as critical states and phasons. Nevertheless, a systematic understanding of the Landau levels of quasicrystals in the presence of the magnetic field has not been established yet. One of the main obstacles is the complication of the quasiperiodic tilings without periodic length scales, thus it has been thought that the system cannot possess any universal features of the Landau levels. In this paper, contrary to these assertions, we develop a generic theory of the Landau levels for quasicrystals. Focusing on two-dimensional quasicrystals with rotational symmetries, we highlight that quasiperiodic tilings induce anomalous Landau levels where electrons are localized near the rotational symmetry centers. Interestingly, the localization length of these Landau levels has a universal dependence on **n** for quasicrystals with **n**-fold rotational symmetry. Furthermore, macroscopically degenerate zero-energy Landau levels are present due to the chiral symmetry of the rhombic tilings. In this case, each Landau level forms an independent island where electrons are trapped at given fields, but with field control, the interference between the islands gives rise to an abrupt change in the local density of states. Our work provides a general scheme to understand the electron localization behavior of the Landau levels in quasicrystals.

DOI: 10.1103/PhysRevB.105.045146

I. INTRODUCTION

Quasicrystals (QCs), long-range crystalline order without translational symmetry, motivate the intensive search for their unique physical phenomena [1–14]. Of particular interest is the unique rotational symmetries that are forbidden in a conventional crystalline solid. Whereas crystalline systems in two dimensions only permit two-, three-, four-, and sixfold rotational symmetries, quasicrystals can have arbitrary **n**-fold rotational symmetry at the cost of losing the lattice translation symmetry. Although the lack of translational symmetry invalidates applications of the conventional Bloch theorem, alternatively, interesting wave-function properties that are not observable in conventional crystalline systems have been investigated [12,15]. Along with this, unconventional transport properties and magnetic responses have been experimentally observed in these systems. In addition, exotic magnetism and superconductivity have been subsequently observed in these quasicrystalline systems [16–24].

Quasicrystals in the presence of an external magnetic field can exhibit highly nontrivial Landau levels (LLs) since the wave functions cannot be described by the competition between the Fermi wavelength and the magnetic lengths. In this paper, we study the electron localization properties of the LL in general **n**-fold rotational symmetric quasicrystals with rhombic tilings. We find that the Aharonov-Bohm-type destructive interference of the LL leads to strictly localized states of the electron wave functions. This phenomenon has been similarly studied in the context of the Aharonov-Bohm cage in crystalline systems [25,26]. However, for the quasiperiodic case, exotic tiling patterns make a unique formation of islands for electron localization and possible interference between the islands via control of the external magnetic field.

Our key results show that the LL wave functions for a vertex model on rotational symmetric QCs with rhombic tiling are strictly localized [31,32] within a certain radius l_k at the rotation centers of the QCs as shown in Fig. 1. This radius l_k is only dependent on n for the n-fold rotational symmetric QCs as

$$l_k = l\frac{\sin\pi(k+1)/n}{\sin\pi/n}, \tag{1}$$

where l is the unit length of the rhombus of the QC. k is an integer which labels distinct localization lengths and magnetic fluxes. Depending on the order of rotations n, the number of localization lengths is uniquely determined as shown in Figs. 1(a)–1(c) and Table I. The well-known Penrose tiling and Ammann-Beenker tiling also belong to this category with $n = 5$ and $n = 8$, respectively, as shown in Figs. 1(a) and 1(b). Moreover, we show that the effective chiral symmetry of the rhombic tiling of QCs ensures macroscopically degenerate zero-energy LLs, where strictly localized electrons form independent islands near the rotational symmetric centers of QCs. With magnetic field control, interference between these islands occurs, resulting in an abrupt change in the local density of states [see Figs. 1(d) and 1(e)].

*junmo1996@kaist.ac.kr
†moonjippark@ibs.re.kr
‡sungbin@kaist.ac.kr

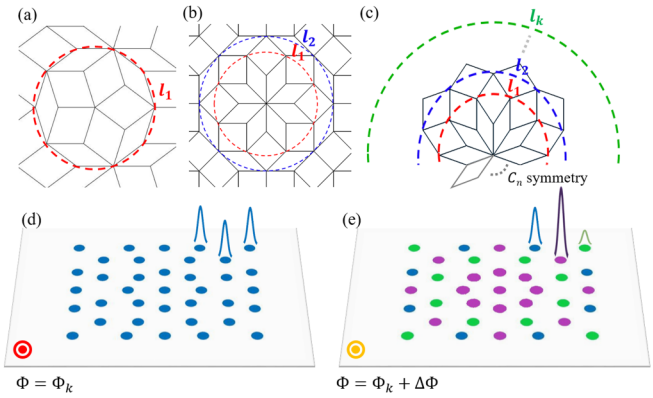

FIG. 1. Schematic figure of the localization radius for the Landau levels emerging in (a) Penrose tiling ($n = 5$), (b) Ammann-Beenker tiling ($n = 8$), and (c) general n-fold rotational symmetric quasicrystals with rhombic tiling. The Landau levels for strict electron localization with localization radius l_k emerge at the flux Φ_k. (d) The wave functions of the localized Landau levels arise near the local rotation symmetry centers of the quasicrystals. Hence they form independent islands, illustrated by the circles. (e) When the flux deviates from Φ_k, the interference between localized islands enhances the localization. The different colored circles imply different amplitudes of the wave functions on each island.

II. GENERIC QUASICRYSTALS

We start our discussion by illustrating generic n-fold rotational symmetric QCs with rhombic tiling. The tight-binding model is comprised of uniform hopping terms $\sum_{i,j} t|i\rangle\langle j|$, where i and j indicate the two sites connected by the edge of the rhombus in the tiling. Figure 2(b) shows the typical n-fold rotation symmetry centers of the tiling with the classifications of the local sites. Here, X_0-class sites are defined as the local rotation symmetry centers. X_i-class sites with $i = 1, 2, \ldots$ are classified in order of the distance from X_0-class sites [see Fig. 2(b)]. We can also classify different types of rhombuses. An R_1-type rhombus is a rhombus surrounding the X_0-class sites and an R_k-type rhombus with $k > 1$ is defined as a rhombus in order of the distance from the X_0-class sites. Now, we consider the application of a uniform magnetic field perpendicular to a two-dimensional plane by applying the Peierls substitution. It turns out that, at certain fluxes Φ_k defined in Eq. (3), strictly localized LLs emerge where the wave functions perfectly vanish beyond the X_{k+1}-class sites.

Such a strict localization of the LLs can be understood by considering Aharonov-Bohm interference at the rotation symmetry centers. Let us consider a wave function initially localized only at the X_0-class sites. Then, under the time evolution, the wave function propagates along the paths that

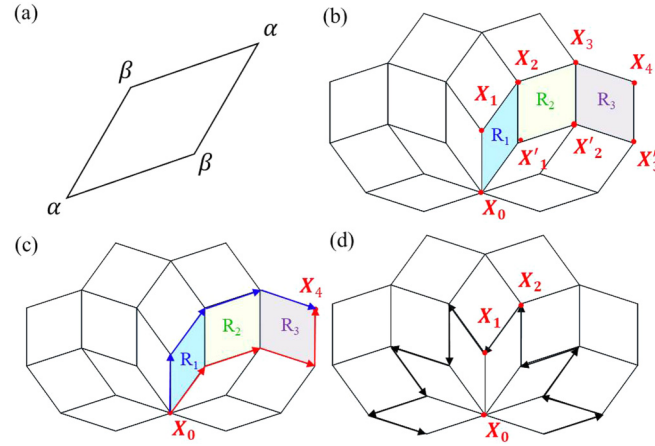

FIG. 2. (a) Bipartition of the sites in a rhombus. Each rhombus in the QCs consists of four sites, which one can separate into two groups G_α and G_β. In the tight-binding model, the sites in G_α can only hop to the sites in G_β and vice versa. (b) Classification of the local site and the rhombus in a generic n-fold rotational symmetric QC. X_0-class sites are defined as the local rotational symmetric centers. X_i-class sites are ith distant sites from the rotation symmetric centers. We define an R_k-type rhombus as a kth distant rhombus from the rotation symmetry center. (c) The paths connecting in between the X_0-class site and X_4-class site exist in pairs (red and blue arrow lines). The combination of those two paths encircles an R_1, R_2, R_3-type rhombus exactly once. (d) Loop consisting of the class X_1 and X_2 sites (black arrow lines).

connect the X_0-class sites and X_k-class sites. Their paths exist in pairs such that the combination of the two paths encircles different types of rhombuses exactly once [for example, the red and blue lines in Fig. 2(c) encircle an $R_1, R_2, \ldots, R_{k-1}$-type rhombus]. Therefore, the perfect destructive interference between the pair of the paths occurs when the flux Φ_k is given as

$$\Phi_k = (2N+1)\pi \frac{1}{\sum_{i=1}^{k} \mathcal{A}_i} = (2N+1)\pi \frac{\sin\frac{\pi}{n}}{l^2 \sin k\frac{\pi}{n} \sin\frac{\pi}{n}(k+1)}. \quad (2)$$

Here, $\mathcal{A}_i$ is the area of an R_i-type rhombus and k is a positive integer smaller than $\frac{n-2}{2}$ (see Supplemental Material Secs. 1 and 2 for the detailed calculations [33]). For the flux Φ_k, the electrons are perfectly localized in between the X_0-class sites and X_k-class sites with the localization radius l_k defined in Eq. (1).

One can use this analysis to find the general condition for the destructive interference for any k values. Table I

TABLE I. Summary of the number of the possible localization lengths l_k as a function of the order of rotations n. For example, in eightfold ($n = 8$) rotational symmetric Ammann-Beenker tiling, the two localization lengths l_1 and l_2 exist. For general n, the number of possible localization lengths is $\frac{(n-3)}{2}$ ($\frac{n}{2} - 2$) when n is an odd (even) integer.

	Penrose [27]	Ammann-Beenker [28]	Unodecagonal [29,30]	Heptadecagonal [29,30]	General
Order of rotations (n)	5	8	11	17	n
Number of localization lengths	1	2	4	7	$\frac{n-3}{2}$ ($\frac{n}{2} - 2$)

summarizes the number of possible localization lengths for several examples of well-known QCs. For larger n, there are more localization length scales. For example, we find that the Penrose tiling ($n = 5$) only has a single localization length, but for the eightfold ($n = 8$) rotational symmetric Ammann-Beenker tiling, two different localization radii l_1 and l_2 exist [see Figs. 1(a) and 1(b)]. For unodecagonal ($n = 11$) and heptadecagonal ($n = 17$) rhombic QCs, on the other hand, four and seven distinct localization length scales exist, respectively. In generic n-fold rotational symmetry, we prove that an n-fold rotational symmetric QC can host $\frac{(n-3)}{2}$ ($\frac{n}{2} - 2$), when n is an odd (even) integer (see Supplemental Material Sec. 3 for details [33]). According to this result, it is worthwhile to point out that, for two-dimensional crystalline systems, $n \leqslant 6$ can only have a single l_k, whereas for general QCs, there can be multiple localization length scales l_k.

With a given flux Φ_k the energy levels of the strictly localized LLs show very interesting characteristics. Regardless of the specific values of Φ_k, there are fixed energy levels. In particular, LLs with the localization length l_1 occur at $E_1 = \pm|t|\sqrt{n}$ or $E_2 = 0$ (see Supplemental Material Sec. 4 for the details [33]). For Φ_2 with l_2, a zero-energy LL with $E_2 = 0$ is present [see Fig. 3(a)]. It is important to note that the emergence of this zero-energy LL is not accidental but originates from the chiral symmetry of the QCs, which will be discussed in the next section.

To exemplify the above general argument, we consider the case of eightfold rotational symmetric Ammann-Beenker (AB) tiling. (Without loss of generality, the same analysis can be applicable for general n-fold rotational symmetric QCs.) For the wave-function propagation from the X_0-class site to the X_2-class site, there exist two paths: $X_0 \to X_1 \to X_2$ and $X_0 \to X_1' \to X_2$. Thus, the amplitude of the wave function at the X_2-class site is determined by the interference effect between the two paths as $|\psi(X_2)| = t|\psi(X_0)|\{1 + \exp[il^2 \sin(2\pi/8)\Phi]\}$, where Φ is the flux per unit area and l is the length of the edge of a rhombus. The wave function at the X_2-class sites vanishes when $\Phi = \Phi_1 \equiv \frac{(2N+1)\pi}{l^2 \sin(2\pi/8)}$, where $N \in \mathbb{Z}$. As a result, the LL is strictly localized in the radius $l_1 = 2l \cos\frac{\pi}{8}$, which is one of the simple examples of Eq. (1) for $n = 8$. The wave functions of the LLs in the AB tiling can be confined within the larger distance, in between the X_0-class sites and X_3-class sites. By calculating all the possible paths that connect from the X_0-class site to X_3-class sites, we find that the LLs are strictly localized within the radius $l_2 = l(1 + 2\cos\frac{2\pi}{8})$ at the flux, $\Phi_2 \equiv \frac{(2N+1)\pi}{l^2 \sin(2\pi/8)} \frac{1}{(1+2\cos\frac{2\pi}{8})}$, where $N \in \mathbb{Z}$.

III. ZERO-ENERGY LANDAU LEVELS

The effective chiral symmetry ensures a particle-hole symmetric energy spectrum of generic n-fold rotational symmetric QCs with rhombic tiling. In rhombic tiling, each rhombus consists of four sites, as shown in Fig. 2(a). In the tight-binding model, one can group the four sites into two distinct groups, each site of which can only hop to sites in the other group. We call the two groups G_α and G_β, respectively, and the tight-binding model Hamiltonian can be written in the following form as

$$H_{\text{bip}} = \sum_{i_\alpha \in G_\alpha, j_\beta \in G_\beta} t_{i_\alpha j_\beta} |i_\alpha\rangle\langle j_\beta| + t^*_{i_\alpha j_\beta} |j_\beta\rangle\langle i_\alpha|, \tag{3}$$

where $t_{i_\alpha j_\beta}$ is the hopping term that connects between the i_α site in G_α and the j_β site in G_β. In this form of the Hamiltonian, the effective chiral symmetry operator Ξ is exactly defined as $\Xi \equiv \sum_{i_\alpha \in G_\alpha} |i_\alpha\rangle\langle i_\alpha| - \sum_{i_\beta \in G_\beta} |i_\beta\rangle\langle i_\beta|$. The Hamiltonian H_{bip} preserves the chiral symmetry by satisfying the following condition, $\{\Xi, H\} = 0$. For any eigenstate $|\psi_E\rangle$ with energy E, we can define the eigenstate $\Xi|\psi_E\rangle$ with the negative energy $-E$ since it satisfies $H\Xi|\psi_E\rangle = -\Xi H|\psi_E\rangle = -E\,\Xi|\psi_E\rangle$. As a result, the energy spectrum of the LLs in the QCs with rhombic tiling is particle-hole symmetric.

Furthermore, chiral symmetry ensures the existence of zero-energy LLs at any l_k. Here, we only provide the sketch

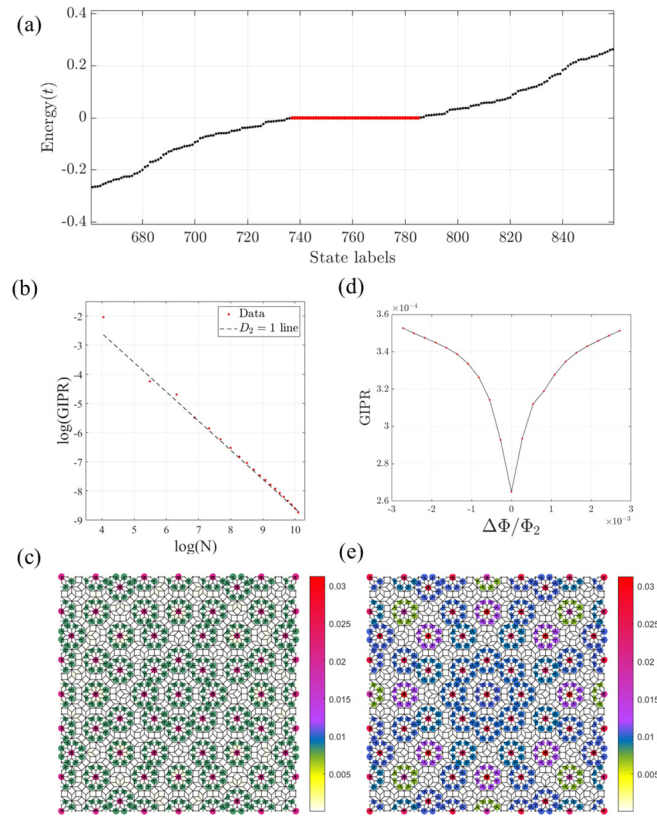

FIG. 3. (a) Energy levels of the LLs at $\Phi = \Phi_2$. We find the zero-energy strictly localized LLs with localization length l_2 (red lines). (b) The zero-energy GIPR at $\Phi = \Phi_2$ as a function of the system size. The strictly localized LLs have a fractal dimension $D_2 = 1$, indicating that the wave functions are extended. For each zero-energy LL, it forms an island near the rotation symmetry center and the number of such islands is macroscopically increasing with system size. (d) GIPR as a function of the magnetic flux. With magnetic flux change, the GIPR increases, indicating the enhancement of the localization. (c), (e) The real-space distribution of the zero-energy LDOS at (c) $\Delta\Phi/\Phi_2 = 0$ and (e) $\Delta\Phi/\Phi_2 = 10^{-3}$. (c) The LDOS is strictly localized at the X_3-class sites. Each rotation symmetry center has the same LDOS amplitude. (e) When the flux is varied, strict localization fails. Interference between the islands occurs and the wave function has different LDOS amplitudes.

of the proof for $k = 2$ and the rigorous proof for the general values of k is provided in Supplemental Material Sec. 4 [33]. The Schrödinger equation for strictly localized LLs with the localization length l_2 can be written as follows,

$$\begin{pmatrix} 0 & T_{01}^{\dagger} & 0 \\ T_{01} & 0 & T_{12}^{\dagger} \\ 0 & T_{12} & 0 \end{pmatrix} \begin{pmatrix} \psi_{X_0} \\ \psi_{X_1} \\ \psi_{X_2} \end{pmatrix} = E \begin{pmatrix} \psi_{X_0} \\ \psi_{X_1} \\ \psi_{X_2} \end{pmatrix}, \tag{4}$$

where T_{IJ} represents the hopping matrix from the I-class sites to J-class sites. ψ_{X_i} indicates the vector of the wave functions at the X_i-class sites. The chiral symmetry constrains $\psi_{X_1} = 0$ but $\psi_{X_0} \neq 0$ for the zero-energy wave function. Then, the linear equations in Eq. (4) host a zero-energy solution if and only if the matrix $T_{12}^{\dagger}$ of the left-hand side is invertible. Using the standard Gaussian elimination method, we find that the matrix becomes noninvertible only if the following condition is satisfied,

$$1 + (-1)^{(n-1)} e^{i\mathcal{A}_{\text{loop},2}\Phi} = 0, \tag{5}$$

where $\mathcal{A}_{\text{loop},2}$ is the area of the loop that consists of X_1-class sites and X_2-class sites. The above equation is valid only if Φ/Φ_1 is a rational number. Since Φ_2/Φ_1 is an irrational number, the above condition is not satisfied. Therefore, strictly localized zero-energy LLs exist. For $k \neq 2$, one can also check the invertibility using the Gaussian elimination methods.

IV. MACROSCOPIC DEGENERACY

Now let us quantify the localization behavior in a generic magnetic flux. We calculate the generalized inverse participation ratio (GIPR), which is defined as $\text{GIPR}(\omega) \equiv \sum_i \rho(i,\omega)^2 / [\sum_i \rho(i,\omega)]^2$, where $\rho(i,\omega)$ is the local density of states at the ith site with the energy ω. The dependence of the system size N characterizes the multifractality of the wave functions by $\text{GIPR}(\omega) \propto N^{-D_2}$, with the fractal dimension D_2; $D_2 = 0$ corresponds to the localized states, $D_2 = 1$ corresponds to the extended states, and $0 < D_2 < 1$ indicates the multifractal critical states [34]. Figure 3(b) shows the calculated GIPR of the AB tiling at zero energy as a function of the system size. Interestingly, we find that the fractal dimension of the strictly localized LLs corresponds to $D_2 = 1$, i.e., the extended states. This indicates that, although the LLs are strictly localized at the rotation symmetry centers, the number of such rotation symmetry centers proportionally increases with the system size. Thus, one can imagine that the strictly localized zero-energy LLs form an island near each rotation symmetry center and a macroscopic number of such islands exist as shown in Fig. 3(c), which is also illustrated in Fig. 1(d). The emergence of macroscopic LLs is the unique feature of rotational symmetric QCs.

As the magnetic flux is slightly changed from Φ_2, strict localization fails, and the wave functions of the LLs extend beyond each island. Figure 3(d) shows the GIPR as a function of the magnetic field. By slightly changing the flux $\Phi = \Phi_2 + \Delta\Phi$, the GIPR rather increases, which indicates the enhancement of the localizations, resulting in an abrupt change in the local density of states (LDOS). Thus, the GIPR has local minima at $\Phi = \Phi_2$. To understand the enhancement of the localization, we compare the LDOS at Φ_2 and $\Phi_2 + \Delta\Phi$ [Figs. 3(c) and 3(e)]. Figure 3(c) shows an identical LDOS amplitude in each rotational symmetric center. This is a consequence of the strict localization of wave functions forming independent islands with Φ_2. In contrast, Fig. 3(e) shows that each rotational center has a different LDOS amplitude. It indicates the onset of interference between the islands that enhances the GIPR.

V. DISCUSSIONS AND CONCLUSION

To summarize, we theoretically demonstrate anomalous strictly localized LLs on rotational symmetric QCs with rhombic tiling. We show that noncrystallographic rotational symmetries [3] generate multiple strictly localized radii l_k. Furthermore, we show that the chiral symmetry of the rhombic tiling QCs gives rise to macroscopically degenerated zero-energy LLs for any l_k. As a result, under special magnetic fields, independent islands are formed by these strictly localized electrons. By controlling the magnetic field strength, we find that the interference between the islands enhances the amount of localization in terms of an increase in GIPR. We emphasize that our general works on rhombic tiling QCs indeed illustrate anomalous LLs that are forbidden in conventional crystalline systems as shown in Table I. Furthermore, the exotic tiling pattern of QCs induces a unique formation of the islands for strictly localized LLs and their interferences as illustrated in Fig. 1.

ACKNOWLEDGMENTS

This work is supported by National Research Foundation Grants No. NRF-2021R1A2C1093060 and No. NRF-2020R1A4A3079707. M.J.P. acknowledges financial support from the Institute for Basic Science in the Republic of Korea through the project IBS-R024-D1.

[1] M. L. Cohen and S. G. Louie, *Fundamentals of Condensed Matter Physics* (Cambridge University Press, Cambridge, U.K., 2016).

[2] J. Kellendonk, D. Lenz, and J. Savinien, *Mathematics of Aperiodic Order*, Progress in Mathematics (Springer, Basel, 2015).

[3] *Aperiodic Order: Volume 2, Crystallography and Almost Periodicity*, edited by M. Baake and U. Grimm, Encyclopedia of Mathematics and its Applications Vol. 166 (Cambridge University Press, Cambridge, U.K., 2017).

[4] *Structure and Properties of Aperiodic Materials*, edited by Y. Kawazoe and Y. Waseda, Advances in Materials Research Vol. 5 (Springer, Berlin, 2003).

[5] *Quasicrystals: An Introduction to Structure, Physical Properties and Applications*, edited by J.-B. Suck, M. Schreiber,

and P. Häussler, Springer Series in Materials Science Vol. 55 (Springer, Berlin, 2013).

[6] J. J. Hauser, H. S. Chen, and J. V. Waszczak, Magnetic properties of Al-Si-Mn and Al-Mn quasicrystals and amorphous films, Phys. Rev. B **33**, 3577 (1986).

[7] S. Poon, Electronic properties of quasicrystals an experimental review, Adv. Phys. **41**, 303 (1992).

[8] Z. V. Vardeny, A. Nahata, and A. Agrawal, Optics of photonic quasicrystals, Nat. Photonics **7**, 177 (2013).

[9] P. Steinhardt and S. Ostlund, *The Physics of Quasicrystals* (World Scientific, Singapore, 1987).

[10] C. Janot, *Quasicrystals: A Primer*, Monographs on the Physics and Chemistry of Materials (Oxford University Press, Oxford, U.K., 2012).

[11] N. Wang, H. Chen, and K. H. Kuo, Two-Dimensional Quasicrystal with Eightfold Rotational Symmetry, Phys. Rev. Lett. **59**, 1010 (1987).

[12] M. Kohmoto, Electronic states of quasiperiodic systems: Fibonacci and Penrose lattices, Int. J. Mod. Phys. B **01**, 31 (1987).

[13] D. DiVincenzo and P. Steinhardt, *Quasicrystals: The State of the Art*, Series on Directions in Condensed Matter Physics (World Scientific, Singapore, 1999).

[14] J. Jeon and S. Lee, Topological critical states and anomalous electronic transmittance in one-dimensional quasicrystals, Phys. Rev. Research **3**, 013168 (2021).

[15] N. Macé, A. Jagannathan, P. Kalugin, R. Mosseri, and F. Piechon, Critical eigenstates and their properties in one- and two-dimensional quasicrystals, Phys. Rev. B **96**, 045138 (2017).

[16] A. I. Goldman, Magnetism in icosahedral quasicrystals: current status and open questions, Sci. Technol. Adv. Mater. **15**, 044801 (2014).

[17] Y. E. Kraus, Y. Lahini, Z. Ringel, M. Verbin, and O. Zilberberg, Topological States and Adiabatic Pumping in Quasicrystals, Phys. Rev. Lett. **109**, 106402 (2012).

[18] R. Chen, C.-Z. Chen, J.-H. Gao, B. Zhou, and D.-H. Xu, Higher-Order Topological Insulators in Quasicrystals, Phys. Rev. Lett. **124**, 036803 (2020).

[19] C.-B. Hua, R. Chen, B. Zhou, and D.-H. Xu, Higher-order topological insulator in a dodecagonal quasicrystal, Phys. Rev. B **102**, 241102(R) (2020).

[20] D. Varjas, A. Lau, K. Pöyhönen, A. R. Akhmerov, D. I. Pikulin, and I. C. Fulga, Topological Phases without Crystalline Counterparts, Phys. Rev. Lett. **123**, 196401 (2019).

[21] Q.-B. Zeng, Y.-B. Yang, and Y. Xu, Topological phases in non-Hermitian Aubry-André-Harper models, Phys. Rev. B **101**, 020201(R) (2020).

[22] H. Huang and F. Liu, Comparison of quantum spin Hall states in quasicrystals and crystals, Phys. Rev. B **100**, 085119 (2019).

[23] F. Barrows, V. Brajuskovic, A. K. Petford-Long, and C. Phatak, Emergent magnetic ordering and topological frustration in quasicrystal artificial spin ices, Phys. Rev. B **99**, 094424 (2019).

[24] J. Jeon and S. Lee, Pattern-dependent proximity effect and Majorana edge mode in one-dimensional quasicrystals, arXiv:2108.02212.

[25] J. Vidal, R. Mosseri, and B. Douçot, Aharonov-Bohm Cages in Two-Dimensional Structures, Phys. Rev. Lett. **81**, 5888 (1998).

[26] S. Mukherjee, M. Di Liberto, P. Öhberg, R. R. Thomson, and N. Goldman, Experimental Observation of Aharonov-Bohm Cages in Photonic Lattices, Phys. Rev. Lett. **121**, 075502 (2018).

[27] D. Austin, Penrose tiles talk across miles, American Mathematical Society: feature column (2005), http://www.ams.org/publicoutreach/feature-column/fcarc-penrose.

[28] F. P. M. Beenker, Algebraic theory of non-periodic tilings of the plane by two simple building blocks: a square and a rhombus, EUT report, WSK, Department of Mathematics and Computing Science (Eindhoven University of Technology, Eindhoven, 1982).

[29] B. Grünbaum and G. C. Shephard, *Tilings and Patterns* (Courier Dover, New York, 1987).

[30] A. Schoen, Infinite tilings, https://schoengeometry.com/c-infintil.html.

[31] M. Oktel, Strictly localized states in the octagonal Ammann-Beenker quasicrystal, Phys. Rev. B **104**, 014204 (2021).

[32] T. Fujiwara, M. Arai, T. Tokihiro, and M. Kohmoto, Localized states and self-similar states of electrons on a two-dimensional Penrose lattice, Phys. Rev. B **37**, 2797 (1988).

[33] See Supplemental Material at http://link.aps.org/supplemental/10.1103/PhysRevB.105.045146 for the model Hamiltonian, the derivation of the localization flux and length scale formulas, the maximum number of l_k for generic quasicrystals, and the energy levels of strictly localized Landau levels.

[34] S. Roche, G. Trambly de Laissardière, and D. Mayou, Electronic transport properties of quasicrystals, J. Math. Phys. **38**, 1794 (1997).